NEUROSCIENCE

Iterative assay for transposase-accessible chromatin by sequencing to isolate functionally relevant neuronal subtypes

Collin B. Merrill[1]*, Iris Titos[1], Miguel A. Pabon[2], Austin B. Montgomery[2], Aylin R. Rodan[2,3,4,5], Adrian Rothenfluh[1,2,4,6]*

The *Drosophila* brain contains tens of thousands of distinct cell types. Thousands of different transgenic lines reproducibly target specific neuron subsets, yet most still express in several cell types. Furthermore, most lines were developed without a priori knowledge of where the transgenes would be expressed. To aid in the development of cell type–specific tools for neuronal identification and manipulation, we developed an iterative assay for transposase-accessible chromatin (ATAC) approach. Open chromatin regions (OCRs) enriched in neurons, compared to whole bodies, drove transgene expression preferentially in subsets of neurons. A second round of ATAC-seq from these specific neuron subsets revealed additional enriched OCR2s that further restricted transgene expression within the chosen neuron subset. This approach allows for continued refinement of transgene expression, and we used it to identify neurons relevant for sleep behavior. Furthermore, this approach is widely applicable to other cell types and to other organisms.

INTRODUCTION

The brain is composed of many distinct types of neurons that form intricate connections across various regions. Each neuron type has specific properties, such as morphology, physiology, or gene expression, that influence local, circuit, and regional function (*1*). Thus, the ability to identify and target specific neurons is critical for understanding the networks and circuits that determine overall brain function. *Drosophila melanogaster* is an excellent model to study fundamental mechanisms in neurobiology because vinegar fly brains consist of approximately 200,000 neurons and are less complex than mammalian brains. Still, even in this "simpler" brain, single or bilateral pairs of neurons can affect behavior (*2*, *3*). Further, neuronal cell type diversity is high, as indicated by the fact that ~22,600 annotated neurons in the connectome fall into ~5600 distinct connectivity types (*4*). These findings underline the need for tools to identify, isolate, and manipulate neurons sparsely and specifically.

Previous large-scale efforts have been made to target groups of neurons in the *Drosophila* brain using stable transgenic lines (*5*, *6*). Most of these methods have relied on shotgun approaches using random fragments or identified promoter regions from genes with known or predicted function in the nervous system fused to an exogenous transcription factor, Gal4 (*6*). Using this approach, thousands of lines have been generated that have proven highly useful to the community. Still, drawbacks from this method include the limited ability to predict which neurons are targeted by this approach, thus necessitating the labor-intensive generation and screening of large numbers of transgenic lines. Furthermore, the collection of generated Gal4 lines includes many diverse neurons, but most lines are still expressed in hundreds of neurons across many distinct cell types (*6*). These findings raise the question of whether a data-driven approach that reveals the cell type–specific chromatin state might be useful to predictably generate tissue-specific tools.

Accessibility of neuronal chromatin is critical for proper gene expression (*7*). Previous single-cell chromatin immunoprecipitation with sequencing (ChIP-seq) and Hi-C studies showed that chromatin accessibility is cell type specific (*8*–*10*), even at the level of cell subtypes (*11*, *12*). Assay for transposase-accessible chromatin by sequencing (ATAC-seq) is an approach that enables detailed and relatively straightforward genome-wide chromatin surveys (*13*). ATAC-seq has been used to investigate how the chromatin landscape is involved in several cellular processes and diseases (*14*–*18*). Cells in the mouse hippocampus, for example, differ substantially in their chromatin accessibility, even within nominally similar cells such as pyramidal cells, which form distinct clusters when analyzed by single-cell ATAC-seq (*19*). It is less clear whether these differences in chromatin accessibility analyzed using ATAC-seq can be used to generate stable transgenic tools to target neuron subtypes selectively, but sparsely, in the brain.

We performed ATAC-seq to analyze the chromatin landscape between all tissues (whole adult flies) and neurons in the head (mostly the brain) selected by fluorescence-activated nuclear sorting. This analysis identified brain-enriched open chromatin regions (OCRs) that, when subcloned in front of a transgene, drove expression preferentially in the brain, although in distinct subsets of neurons. Conversely, whole body–enriched OCRs drove transgene expression largely outside the brain. Different brain-enriched OCR transgenes affected sleep behaviors when the OCR-expressing neurons were activated. To home in on the neurons responsible for a selected behavioral phenotype, we performed a second, iterative round of ATAC-seq specifically from round one transgene-expressing neurons that affected the selected phenotype. Subcloned round two OCR2s that were enriched compared to all neurons identified subsets of round one neurons that affected the selected behavioral phenotype when using intersectional genetics. Our results demonstrate that an iterative

[1]Department of Psychiatry, Huntsman Mental Health Institute, University of Utah, Salt Lake City, UT 84108, USA. [2]Molecular Medicine Program, University of Utah, Salt Lake City, UT 84112, USA. [3]Division of Nephrology and Hypertension, Department of Internal Medicine, University of Utah, Salt Lake City, UT 84132, USA. [4]Department of Human Genetics, University of Utah, Salt Lake City, UT 84112, USA. [5]Medical Service, Veterans Affairs Salt Lake City Health Care System, Salt Lake City, UT, USA. [6]Department of Neurobiology, University of Utah, Salt Lake City, UT 84112, USA.
*Corresponding author. Email: collin.merrill@utah.edu (C.B.M.); adrian.rothenfluh@hsc.utah.edu (A.R.)

ATAC-seq approach can be used to isolate specific neuron subtypes that underlie distinct behavioral phenotypes in an informed manner. This data-driven approach thus provides an efficient technique to create genetic tools to identify and investigate the function of new neuronal populations that is translatable to other organisms and other tissues of interest.

RESULTS

OCRs drive tissue-specific gene expression

Gene expression is often used to define cell populations within complex tissues. In the brain, for example, inhibitory neurons are often identified by expression of marker genes for γ-aminobutyric acid (GABA) signaling, such as *Gad1* or *vGAT*. Still, these markers are widely expressed in various cell subtypes, with active gene regulatory elements in enhancers providing spatial specificity to marker gene promoter activity (*20*, *21*). Thus, we asked whether active OCRs outside of gene promoters would be able to drive gene expression. To answer this question and to ascertain whether OCR-driven gene expression could be done in a tissue-specific manner, we assayed OCRs in two very broad tissues—whole flies and neurons isolated from fly heads—using ATAC-seq.

We leveraged the *Gal4/UAS* system (*22*) to drive nuclear green fluorescent protein (GFP) expression in whole flies using two independent whole-organism drivers (*Tubulin84B-Gal4* and *Actin5c-Gal4*; approximately 250 flies per sample, four samples per driver, eight total whole-fly samples) and two neuron-specific drivers (*elav-Gal4* and *nsyb-Gal4*; approximately 250 flies per sample, four samples per driver, eight total neuron samples). We isolated GFP-expressing nuclei from whole flies or from head neurons using fluorescence activated nuclei sorting, as described previously (*23*). The isolated nuclei were then used to generate ATAC-seq libraries. When we compared chromatin accessibility between whole flies and head neurons using unsupervised hierarchical clustering, the eight samples grouped into two clear classes: head neurons and whole flies, with many more accessible OCRs observed in head neurons compared to whole flies (Fig. 1A).

To determine whether specific gene regions or features were enriched in neuron-specific OCRs, we annotated each OCR (e.g., promoters, exons, introns, etc.) and calculated the proportion of OCRs annotated to each genomic feature type. We then compared the proportion of each feature in wholefly and neuron OCRs. We found that the proportion of several feature types that typically contain regulatory sequences, including enhancers [2 to 3 kb from the transcription start site (TSS) and 1 to 2 kb from the TSS], 5′ untranslated regions (UTRs), exons, first introns, other introns, and 3′ UTRs were significantly higher in neurons compared to whole flies, while distal intergenic regions were lower (Fig. 1B). The increased proportions we observed for the enriched features in neurons suggests that these OCR types are particularly relevant for neuronal cell type–specific gene expression.

We next performed differential accessibility analysis on OCRs from whole flies and neuron samples. From the 16,337 consensus OCRs identified by pooling all wholefly and head neuron libraries, we identified 12,988 differential OCRs. Of these, 439 were significantly more accessible in whole flies and 12,548 were more accessible in neurons (Fig. 1C). Because enhancers and first introns often contain regulatory elements in *Drosophila* (*24*, *25*), we selected OCRs using the following criteria: *OCR*s with the largest $\log_2$ fold change, *OCR* distance >500 base pair (bp) from the TSS, and *OCR* location within the first intron or within an enhancer 2 to 3 kb upstream of the TSS. These criteria suggested eight candidate OCRs from whole flies and eight OCRs from neurons (16 total OCRs; Fig. 1, D to F). We subcloned the differentially accessible OCRs upstream of a minimal *Drosophila* synthetic core promoter (*DSCP*) (*5*) coupled to *Gal4* and injected the plasmids into fly embryos for insertion at the same genomic locus (*26*) to generate stable transgenic *OCR-Gal4* fly lines. We named each line using the chromosome arm and last three digits of the sequence coordinate of the subcloned OCR (i.e., the peak located at 3R:9490745-9491579 was named *3R579*). Of the embryos injected with *OCR-DSCP-Gal4*–containing plasmids, we obtained five neuron OCR-derived lines (*2L722*, *3R579*, *X688*, *2R038*, and *3L858*) and two whole-fly OCR lines (*2R131* and *3R634*). Some injected *OCR-Gal4* plasmids (mostly whole fly–derived OCRs) did not yield stable transgenic lines, so we therefore repeated the OCR cloning approach using an *HSP70* minimal promoter instead (*27*). This yielded an additional two neuron-derived OCR lines (*3L018* and *2L631*) and two whole-fly OCR lines (*3L772* and *2L009*). Together, we generated 11 stable *OCR-Gal4* fly lines: 7 were derived from regions with increased chromatin accessibility in neurons and 4 were from whole flies.

Differentially accessible chromatin regions drive tissue-specific transgene activity

To test whether differentially accessible OCRs drive tissue-specific *Gal4* expression, we first evaluated whole-body expression using a *UAS-GFP* reporter (Fig. 2A and fig. S1). Three *whole fly-OCR-Gal4* lines drove obvious-to-strong GFP expression in fly bodies, while *neuron-OCR-Gal4* lines all showed very dim GFP expression. Quantifying the GFP intensity (outside of the head) showed significantly higher expression in the bodies of *whole fly-OCR-Gal4* flies ($P = 0.0006$; $W = 214$, Wilcoxon signed-rank test; Fig. 2B). Similar results were obtained from whole-body sections stained with X-gal (from *OCR-Gal4;UAS-lacZ* flies; fig. S2). Quantifying the immunostaining intensity showed significantly more signal in brains from *neuron-OCR-Gal4* lines than from *whole fly-OCR-Gal4* lines ($P = 0.003$; $W = 43$, Wilcoxon; Fig. 2C; see Fig. 3 for immunostaining). Together, *whole fly-OCR* lines express more strongly throughout the body, while *neuron-OCR* lines express more strongly in brains (Fig. 2D).

Brain-specific OCRs drive transgene expression in distinct neurons

Next, we examined transgene expression in the brain using a membrane-bound V5-tagged marker (*28*) driven by *OCR-Gal4* and performing immunohistochemistry (Fig. 3A). Controls using the empty *DSCP* vector (*EVD*) or empty *HSP70* promoter (*EVH*) drove very sparse reporter expression (Fig. 3B), while each of the seven *neuron-OCR-Gal4* lines drove V5 expression in several brain compartments, staining from thousands to tens of neurons (Fig. 3C). Conversely, *whole body-OCR-Gal4* lines drove markedly less V5 expression in the brain, with two of the four lines showing no staining (*2R131* and *3R634*; Fig. 3D). The two *whole fly-OCR-Gal4* lines that showed expression in the brain (*3L772* and *2L009*) were both generated using vectors containing the *HSP70* minimal promoter. Adding a *whole fly-OCR* recapitulated some empty vector staining (such as the fan-shaped body in *3L772*), drove marker expression in additional areas (such as antennal lobe projection neurons in *2L009*), and subtracted some marker expression driven by the empty vector (i.e., antennal lobe intrinsic neurons that are absent in *3L772* and

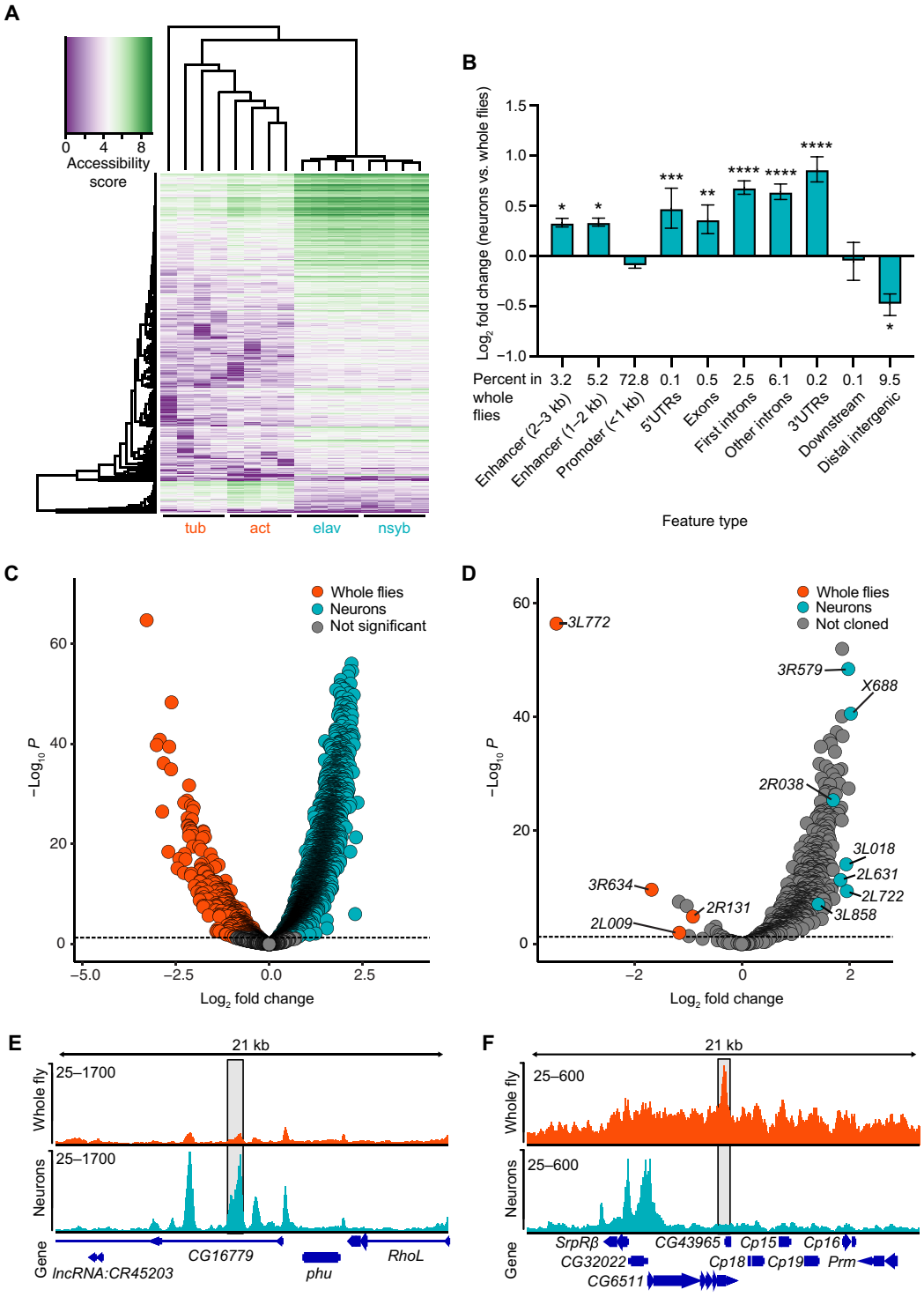

Fig. 1. Differential chromatin accessibility between neurons and whole flies. (**A**) Heatmap of chromatin accessibility in GFP-positive nuclei from whole flies (*Tubulin84B-Gal4* and *Actin5c-Gal4* drivers) and neurons from detached heads (*elav-Gal4* and *nsyb-Gal4* drivers). Each row represents a specific OCR. Purple, decreased accessibility; green, increased accessibility. Each driver was analyzed using four biological replicates. (**B**) Fold difference for fraction of OCRs annotated to each feature type in neurons compared to whole flies. The data were analyzed using one-way analysis of variance (ANOVA) followed by Holm-Sidak multiple comparisons tests. *$P < 0.05$, **$P < 0.01$, and ***$P < 0.001$ compared to whole flies. (**C**) Volcano plot showing differentially accessible OCRs from whole flies (orange) or neurons (cyan). The dotted line represents $P = 0.05$. (**D**) Differentially accessible OCRs annotated to first intron or enhancer regions in whole flies ($\log_2$ fold change < 0) and neurons ($\log_2$ fold change > 0). The orange and cyan dots represent whole fly–and neuron-derived OCRs, respectively, that were used for subcloning experiments. (**E** and **F**) Representative OCRs with increased accessibility in (E) neurons within gene *CG16779* and (F) whole flies within gene *CG43965*. The shaded area indicates the representative OCRs, and numbers on the left indicate the scale of the *y* axis in read count.

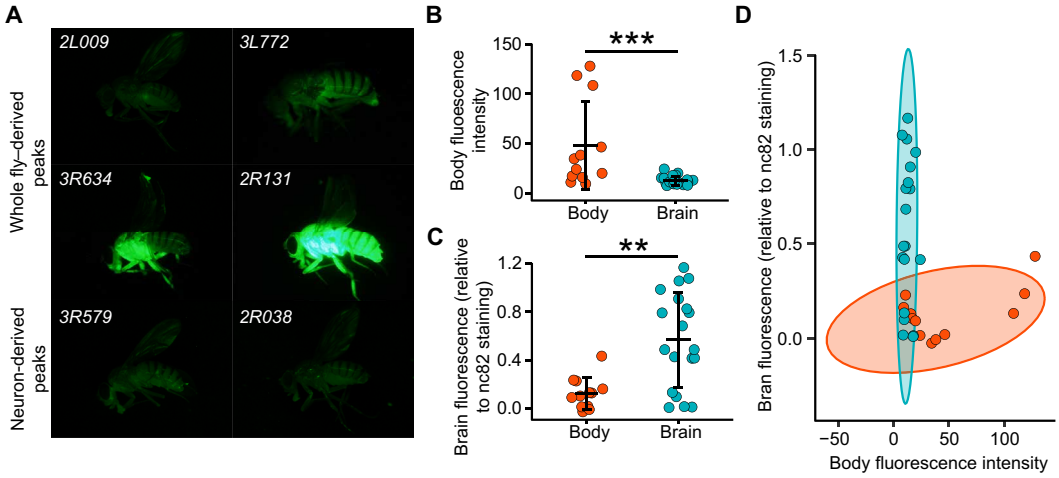

Fig. 2. Chromatin regions that are more open in whole flies drive transgene expression in the fly body rather than the brain. (**A**) Whole fly-derived OCR (*2L009*, *3L772*, *3R634*, and *2R131*) fragments drive Gal4 expression, which then activates *UAS-GFP*. GFP fluorescence is obvious in the body, while representative neuron-derived OCRs (*3R579* and *2R038*) drive little GFP in whole bodies. (**B**) Quantification of GFP fluorescence in the body driven by whole fly–(orange) or neuron-derived (cyan) OCRs. (**C**) Quantification of reporter expression in the brain driven by the distinct OCR-transgenes. $^{**}P = 0.003$; $n = 12$ for whole-fly peaks and $n = 12$ for neuron-derived peaks. (**D**) GFP fluorescence driven by whole fly–versus neuron-derived OCRs for each OCR. $^{***}P = 0.0006$; $n = 12$ for whole-fly peaks and $n = 19$ for neuron-derived peaks. The data in (B) and (C) represent means ± SD and were compared using Wilcoxon signed-rank tests. The fluorescence for immunostained reporters in the brain was normalized to nc82 reference staining.

2L009), suggesting that the subcloned OCR regions contain instructive and repressive activity.

Aside from the striking difference in the number of neurons observed in *neuron-OCR-Gal4* lines, the staining patterns of these seven lines were very diverse, with many labeled neurons expressed in distinct anatomical regions in one, but not other lines (e.g., the mushroom bodies in *X688*, the ellipsoid body in *2R038*, or the protocerebral bridge in *2L631*). These data show that neuron-derived accessible OCR regions drive expression in distinct subsets of neurons.

Neurons identified by OCRs drive behavioral phenotypes

The *Drosophila Gal4/UAS* system, used here to determine OCR-mediated reporter gene expression, is highly versatile and can be used to drive neuronal effectors, such as *UAS-TrpA1*, which allows for temperature-dependent neuronal activation at increased temperature (~29°C) (*29*). Because we are interested in how individual neurons affect complex behaviors, we investigated how the *OCR-Gal4* neurons derived from our ATAC-seq analysis affected various sleep parameters. We chose this behavior because sleep is regulated by neural activity (*30*, *31*), can be assessed for various phenotypes (*32*), and different neuron types are involved in sleep regulation (*33*). Of the five sleep parameters measured, only one of the four *whole fly-OCR-Gal4* lines affected one of the five tested parameters (Fig. 4A), while five of the seven *neuron-OCR-Gal4* lines affected one or more parameters each (Fig. 4B). These data are consistent with our brain expression data, given that *neuron-OCR-Gal4* lines express more widely in the brain (Fig. 3) and show that neuron-derived accessible OCRs are more likely to be useful for identifying neurons that modulate behaviors.

Iterative ATAC-seq identifies neuron-specific OCRs that drive transgene expression

The *neuron-OCR-Gal4* line *2L722* is expressed in about 250 central brain neurons spanning many distinct brain regions (Fig. 3C). When these neurons were activated, flies showed increased nighttime sleep (Fig. 4, C to E). Because the goal of our ATAC-seq approach was to develop tools for specific neuronal identification and manipulation, we asked whether we could further subdivide these 250 neurons in a data-driven manner and also identify smaller subpopulations that affect night sleep. *Neuron-OCR-Gal4s* were enriched for neuronal expression but only targeted a subset of neurons. We thus reasoned that the same combination of specificity and sparsity might apply if we performed a second, iterative round of ATAC-seq, i.e., OCRs that were more accessible in *2L722* neurons would drive gene expression in a subset of *2L722* neurons.

To test this hypothesis, we performed ATAC-seq on GFP-labeled nuclei from two different *OCR-Gal4* lines: *2L722* and *3R579*. We detected 33,471 consensus peaks in pooled *2L722-*, *3R579-*, *elav-*, and *nsyb*-derived libraries. Principal components analysis showed that the *2L722* and *3R579* samples clustered distinctly from the neuronal and the whole-fly samples (Fig. 5A). Unsupervised hierarchical clustering showed that the overall chromatin accessibility was different between the whole fly, neuron, *2L722*, and *3R579* samples (Fig. 5B). Similar to the neuron versus whole-body comparison (Fig. 1B), *2L722* and *3R579* neurons showed a higher proportion of OCRs in enhancers, exons, introns, 5′ UTRs, and 3′ UTRs (Fig. 5C), suggesting that these regulatory regions confer increasingly cell type–specific gene expression.

Differential accessibility analysis between *2L722* neurons and neuron-specific libraries (*elav* and *nsyb*) identified 6575 differentially accessible peaks ($P < 0.05$), with 487 peaks more open in *2L722* neurons and 6088 peaks more open in neurons. Comparing *3R579* neurons and whole brains identified 20,721 differentially accessible peaks ($P < 0.05$) in *3R579* libraries compared to neuron libraries, with 6283 more open regions in *3R579* neurons and 14,438 more open regions in neurons. Using the same approach we used to identify candidate OCRs in the first ATAC-seq experiment, we detected 1190 first intron OCR2s (for second round OCR) when comparing

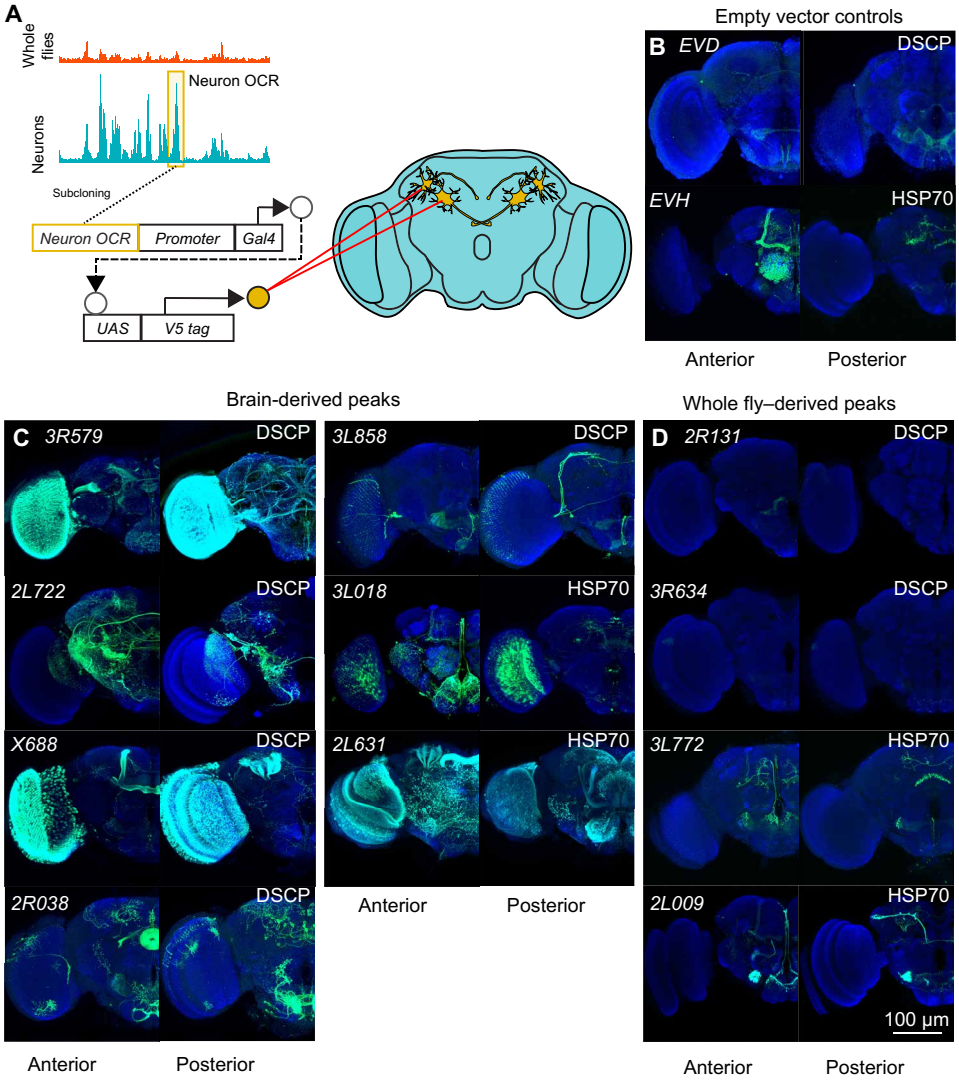

Fig. 3. Neuron-derived OCRs drive transgene expression in different neurons. (**A**) Schematic depicting ATAC-seq-derived *OCR* fragments 5′ to minimal promoters [*Drosophila* synthetic core promoter (*DSCP*) or promoter from the *Hsp70* gene] driving *Gal4*, which then activates a membrane-bound myristoylated V5-tagged marker (encoded by *UAS-myr::smGdP-V5*). (**B** to **D**) Whole brain anti-V5 (green) and neuropil stainings (anti-nc82, blue) of (B) empty vectors containing no OCR fragments but just the promoters 5′ of *Gal4*, (C) neuron-derived OCRs, and (D) whole-body OCRs. The OCR name is shown in the upper left corner of each image, and the promoter is shown in the upper right corner. *EVD* and *EVH* in (B) indicate empty vectors containing the *Drosophila* synthetic core promoter or the minimal *HSP70* promoter, respectively. Scale bar, 100 µm, applicable to all images.

2L722 neurons to whole brains, with 18 significantly more open in *2L722* libraries ($\log_2$ fold change > 0; Fig. 5D). We also detected 1357 differentially accessible first intron OCRs between *3R579* neurons and whole brains ($\log_2$ fold change > 0). Of these, 183 peaks were more open in *3R579* neurons (Fig. 5E). We hypothesized that these second-round OCRs would identify a subset of the original neuron populations. Thus, we selected two and five significantly more accessible intron OCRs (OCR2) from *2L722* and *3R579* libraries ($\log_2$ fold change > 1; Fig. 5F) and generated stable transgenic fly lines. OCR2s were subcloned upstream of the *DSCP* promoter to drive expression of *Flp recombinase* (*FLP*) (*34*), which allowed for an intersectional approach focusing on neurons within the *OCR-Gal4* pattern only. We simultaneously used *2L722-* or *3R579-Gal4* and *OCR2-FLP* to express two reporter genes: (i) a *UAS-GFP* reporter driven by *2L722-Gal4* or *3R579-Gal4* in parental OCR neurons (Fig. 3A) and (ii) a hemagglutinin (HA)–tagged reporter downstream of *UAS* and the *FLP recombinase target (FRT)-STOP-FRT* sequence. Thus, the HA-tagged reporter was expressed only in neurons that simultaneously expressed *2L722-Gal4* or *3R579-Gal4* AND *OCR2-FLP* because *2L722-Gal4*–or *3R579-Gal4*–driven *FLP* expression causes the removal of the transcriptional *STOP* cassette in the *FRT-STOP-FRT-HA* reporter.

We observed sparse HA staining in the *OCR2-FLP∩2L722-Gal4* intersection (Fig. 6, A to E). The staining was variable from fly to fly, likely due to incomplete penetrance of FLP-mediated excision of the *STOP* cassette, since FLP was originally intended to generate mosaic expression (*35*, *36*). Heat-shocking *Drosophila* larvae at 37°C can increase FLP activity and resultant transgene expression (*28*), so we

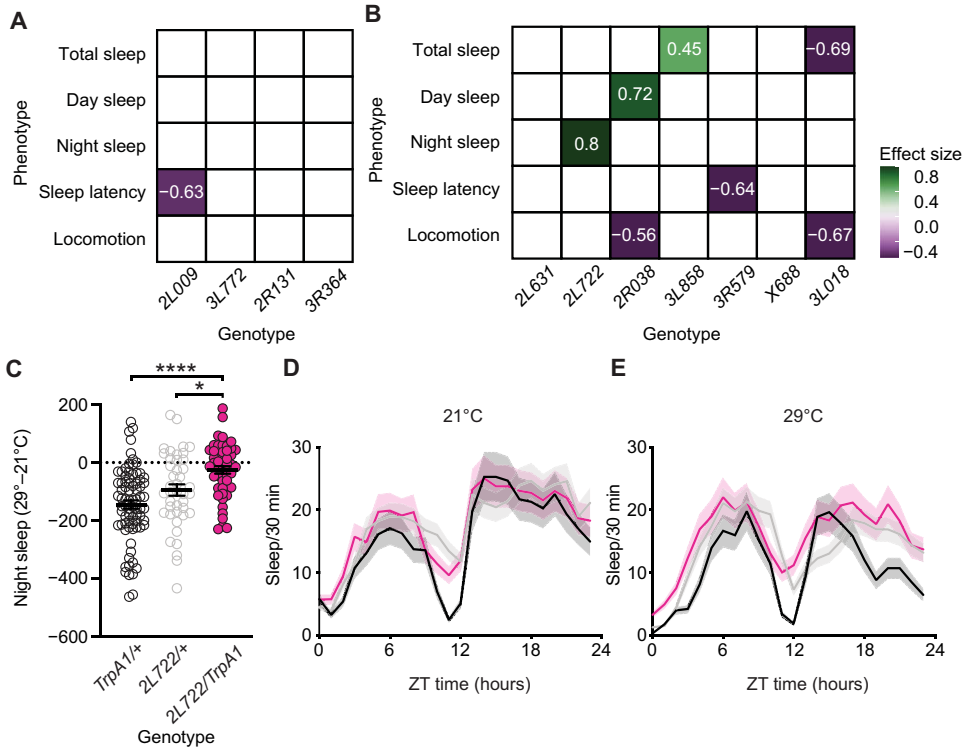

Fig. 4. Neuron-derived OCRs express in neurons affecting diverse sleep phenotypes. Expression of temperature-activated TrpA1 channels (*UAS-TrpA1*) was driven using *OCR-Gal4*. Flies' sleep measures for 2 days at 21°C were compared to the same flies for 2 days at 29°C, which activates TrpA1 and the neurons expressing it. (**A** and **B**) Effects on sleep phenotypes by activating TrpA1 are shown (Hedge's *g* effect sizes are shown where significant, accounted for the effect of temperature in the absence of TrpA1 expression). (A) Whole fly–derived OCRs caused few effects on sleep phenotypes, while neuron-derived OCRs caused diverse sleep phenotypes (B). (**C**) Temperature increases reduced night sleep duration in controls (left two genotypes), but not in *2L722>TrpA1* experimental flies, suggesting that *2L722*-expressing neurons promote night sleep (Kruskal-Wallis test followed by Dunn's multiple comparisons test. $*P = 0.01$ and $****P < 0.0001$). (**D** and **E**) Average sleep-o-grams showing sleep at 21°C (D) and 29°C (E), with SEM shading.

heat-shocked the flies at the larval stage in an attempt to enhance FLP penetrance. This led to improved expression of the HA reporter but expression was still clonal, i.e., often not bilaterally symmetrical and variable from individual fly to fly (of the same genotype). Despite this heterogeneity, we observed distinct intersectional *OCR2-FLP∩2L722-Gal4* staining between the *2R236-FLP* (Fig. 6, B and C), *2L945-FLP* (Fig. 6, D and E), and the control *empty-FLP* (*EVF*), which contained only a minimal *DSCP* promoter (Fig. 6F; $X^2 = 102.4$, $P = 5.19 \times 10^{-18}$, Chi-squared test; fig. S4). *2R236-FLP∩2L722-Gal4* flies showed staining in the posterior dorsolateral protocerebrum projecting toward the protocerebral bridge (Fig. 6, B and C), while *2L945-FLP∩2L722-Gal4* flies showed staining in the ventrolateral protocerebrum and the median bundle (Fig. 6, D and E, and fig. S5). When we examined *OCR2-FLP* staining independent of *2L722-Gal4*, we found that *OCR2-FLP* was expressed in fewer but similar brain regions as *2L722-Gal4*. We also observed some clustered staining where the number of stained nuclei was larger in *OCR2-FLP* than in the *2L722-Gal4* pattern (fig. S6). These data suggest that *OCR2-FLPs* are sparsely expressed, but that they label some neurons that reside outside the parental *2L722-Gal4* pattern. However, this result also suggests that *OCR2s* do indeed label a subset of the parental *2L722-Gal4* pattern, which validates our iterative approach. Furthermore, these results support our intersectional approach, which limited the *OCR2* pattern to a subset exclusively within the *2L722-Gal4* pattern.

In the *OCR2-FLP∩3R579-Gal4* lines, we observed sparse HA staining with some distinct intersectional staining in each *OCR2-FLP∩3R579-Gal4* line (fig. S7). Because of the complexity of the *3R579* expression pattern and the incomplete penetrance of FLP-mediated excision of the STOP cassette in the *OCR2-FLP∩3R579-Gal4* intersection, we were unable to reliably identify neurons stained for each intersection. However, the extant but sparse staining we observed in the *OCR2-FLP∩3R579-Gal4* intersection supports our iterative ATAC-seq approach. Overall, these results show that—as hypothesized—our second round ATAC-seq–derived *OCR2-FLP* lines express transgenes in subsets of the parental OCR neurons and that different *OCR2-FLP* lines are composed of distinct subsets of OCR neurons.

Chromatin regions with increased accessibility identified by iterative ATAC-seq impart subtype-specific behavioral phenotypes

Last, we examined whether the *OCR2-FLP∩2L722-Gal4* intersectional neurons have functional relevance. To do so, we crossed the *2R236-FLP∩2L722-Gal4* and *2L945-FLP∩2L722-Gal4* lines to *UAS-FRT-STOP-FRT-TrpA1*, so that only *FLP-* AND *Gal4*-positive neurons expressed TrpA1, which allowed us to activate *OCR2*-containing intersectional neurons in a temperature-dependent manner. Our hypothesis was that a subset of *2L722* neurons is sufficient to mediate the TrpA1-induced increase in nighttime sleep (Fig. 4).

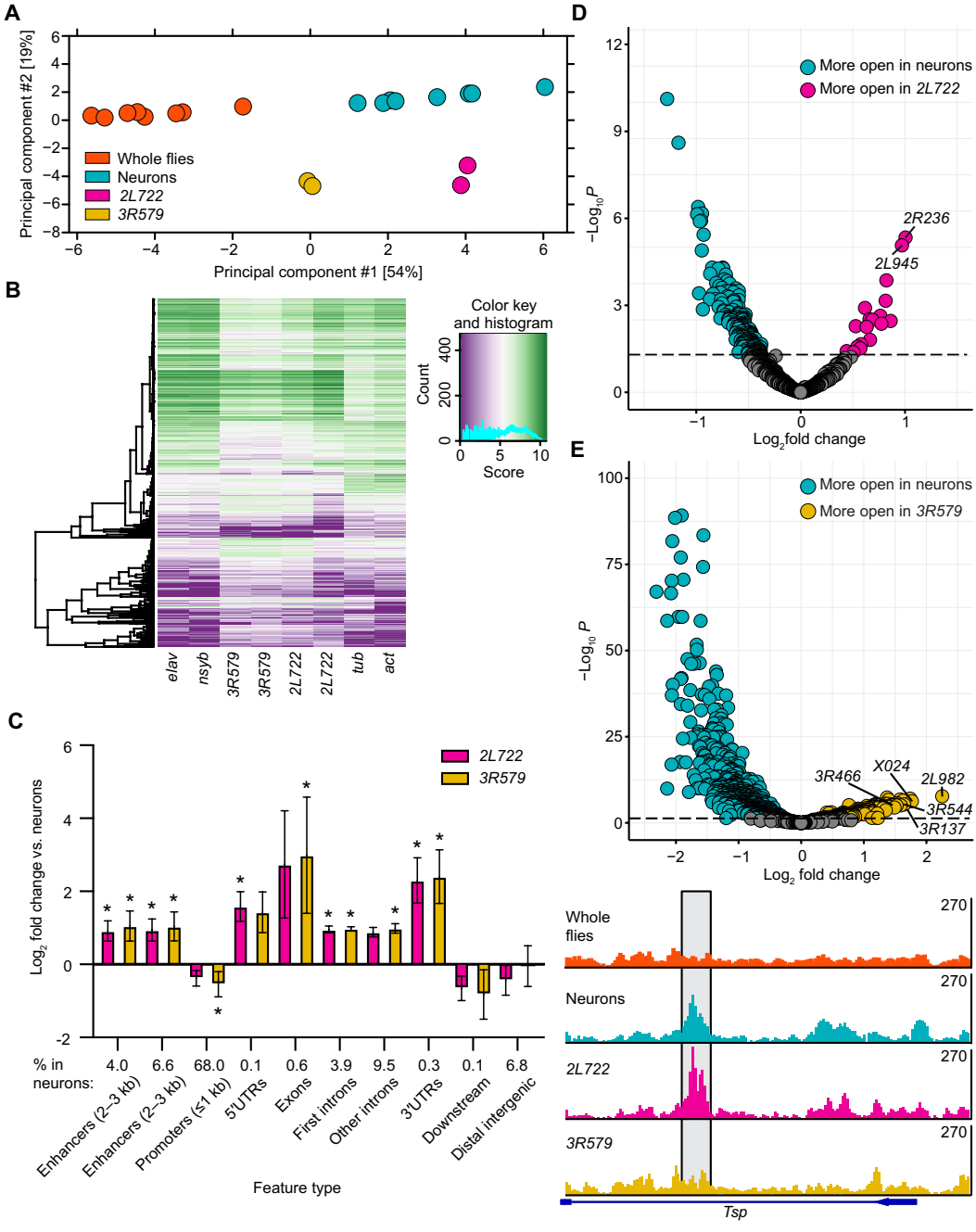

Fig. 5. Iterative ATAC-seq identifies differentially accessible chromatin regions in neuronal subtypes. A second round of iterative ATAC-seq was performed using GFP-positive nuclei from *2L722* and *3R579* neurons. (**A**) Principal components analysis of OCRs from whole flies (orange), brains (cyan), *2L722* neurons (magenta), and *3R579* neurons (yellow). The *x* and *y* axes are scaled by the contribution of each principal component to the overall variability in the dataset. (**B**) Heatmap showing the overall chromatin accessibility between whole flies, brains, *2L722* neurons, and *3R579* neurons. Purple indicates decreased accessibility and green indicates increased accessibility. (**C**) Fold differences in the fraction of OCRs annotated to each genomic feature in *2L722* (magenta) and *3R579* neurons (yellow) compared to the proportion of each genomic feature in head neurons. The data were analyzed using Kruskal-Wallis tests followed by Dunn's multiple comparisons tests, $*P < 0.05$ compared to head neurons. (**D**) Volcano plot showing differentially accessible OCRs in GFP-positive nuclei from neurons (cyan) and *2L722* neurons (magenta). (**E**) Volcano plot showing differentially accessible OCRs in GFP-positive nuclei from neurons (cyan) and *3R579* neurons (yellow). The annotated points in (D) and (E) represent subcloned OCR2s. (**F**) A representative OCR annotated to the first intron of *Tsp* was identified in *2L722* neurons (magenta) and is more accessible than in *3R579* neurons (yellow), neurons (cyan), or in whole flies (orange). The shaded area indicates the OCR.

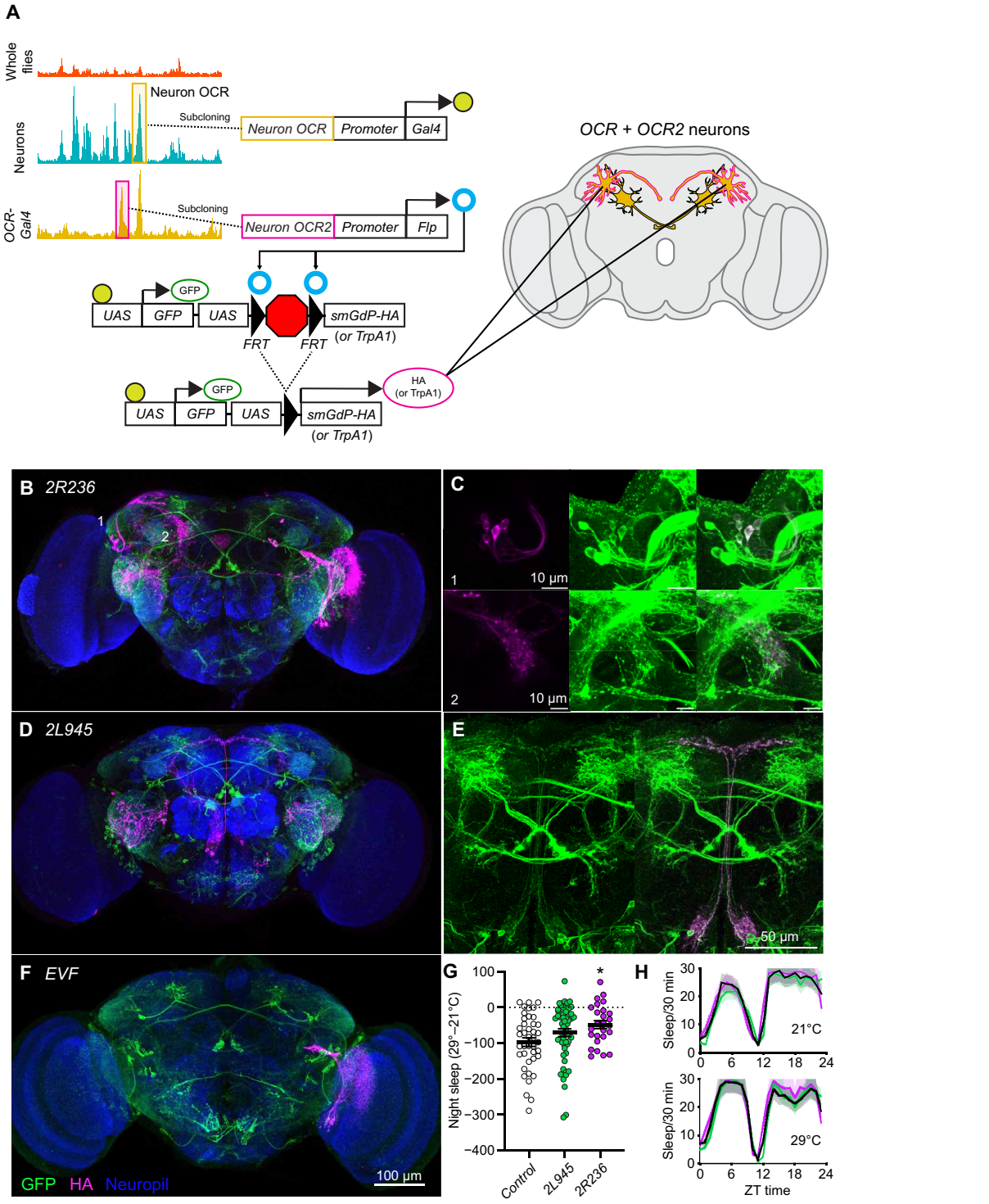

Fig. 6. Differentially-accessible OCRs detected by iterative ATAC-seq drive transgene expression in *2L722* neuron subtypes. (**A**) Schematic depicting the subcloning and genetic strategy. (**B** to **F**) GFP expression (green) driven by first round *2L722-Gal4* and HA expression (magenta) driven in neurons expressing both *2L722-Gal4* and *2L722*-derived iterative *OCR2-FLPs*. Neuropil (nc82) is stained in blue. (B) *2L722∩2R236* neurons. (C) Zoomed images showing the cell bodies (1) and projections (2) of HA-positive lateral horn neurons isolated with *2L722∩2R236* intersectional drivers. (D) *2L722∩2L945* neurons. (E) Zoomed images showing *2L722*-driven GFP only (left) and *2L722∩2L945*-driven HA colocalization in median bundle neurons as well (right). (F) *2L722∩Empty vector FLP* (*EVF*, with *DSCP* promoter), which stains in some optic lobe neurons. (**G**) Temperature increases reduce night sleep duration in controls (black) and *2L722∩2L945*-activated neurons (green) but significantly less so in *2L722∩2R236* neurons (blue), suggesting that these intersectional neurons (B) promote night sleep. **P* = 0.04, Kruskal Wallis test followed by Dunn's multiple comparisons test. (**H**) Average sleep-o-grams showing nighttime sleep at 21° and 29°C.

While *2R945-FLP∩2L722-Gal4* flies had the same night sleep as the *empty-FLP∩2L722-Gal4* controls, *2R236-FLP∩2L722-Gal4* flies showed an increased night sleep phenotype ($F_{2,120} = 3.566$, $P = 0.03$; $^*P = 0.02$, Dunnett's multiple comparisons test; Fig. 6, G and H), which was similar to the increased nighttime sleep phenotype observed in the original *2L722-Gal4;UAS-TrpA1* flies. These results indicate that *2R236-FLP∩2L722-Gal4* neurons, a subset of the original ~250 *2L722* neurons, are involved in promoting night sleep. Thus, our approach of starting with a given tissue (neurons) and performing ATAC-seq to generate specific, but sparse, transgenic lines can be successfully used iteratively to isolate functionally relevant, sparse neuron subpopulations. Further, our approach can be used to isolate many other behaviorally relevant neuronal subpopulations in other tissues or in other organisms.

DISCUSSION

The brain consists of thousands of different cell types, with many yet to be investigated regarding their function. Because of this vast diversity, we need tools—including new approaches for the efficient generation of these tools—to identify and study many of these neuronal cell types. Here, we show that tissue-specific, iterative ATAC-seq is a useful approach to generate these new tools.

We determined genome-wide OCRs for the whole body and for the brain. Many more OCRs were identified in the brain compared to the whole body. When we determined genome-wide OCRs from specific neurons, we again identified more OCRs in specific neurons compared to all neurons. This is likely due to the ATAC-seq signal-to-noise ratio because an OCR that is accessible in a specific subset of neurons may not result in a large enough signal to be detected when surveying all neurons, much less all cells in the body. Similar results were found when comparing mouse bulk cortex to more specific entorhinal cortex data, albeit with data derived from histone mark-specific chromatin immunoprecipitation, which resulted in more enhancers being identified in the more specific tissue (*37*). In our data, the OCRs from more specific tissues encompassed a larger proportion of OCRs in enhancers and throughout the transcriptional unit, while a larger proportion of accessible OCRs were located in promoters in more general tissue samples. This suggests that nonpromoter regions confer tissue-specific gene expression and could be used to generate tools to identify and manipulate subtypes of cells. Enhancer regions are cell specific (*38*) and are critically involved in regulating promoter activity and downstream gene expression (*39*). Single-cell approaches could impart greater specificity in identifying OCRs that are present in sparse neuron subsets (*40*). However, differential OCRs, particularly within neurons of the same type (i.e., GABAergic, dopaminergic, etc.), may be difficult to detect in single-cell analysis.

When we subcloned first intron OCRs that were more accessible in neurons compared to whole flies, we found that they drove transgene and reporter expression preferentially in neurons. Conversely, OCRs that were enriched in whole fly–derived data drove very sparse or no expression in the brain. Thus, OCRs that are enriched in a specific tissue drive expression preferentially in the tissue of interest. This is consistent with mammalian studies showing that tissue-specific ATAC-seq can be used to generate tissue-specific tools. These approaches have yielded viral Adeno-associated virus vectors that express in subsets of GABAergic interneurons starting from GABA neuron-specific ATAC-seq (*41*) or in subsets of the visual cortex starting from adult primary visual cortex single-cell ATAC-seq (*42*). Therefore, tissue-specific ATAC-seq data can be harnessed to generate tissue-specific tools in *Drosophila* and mammals.

Because the neuron-specific transgenes we generated are expressed in tens to thousands of neurons, we re-applied the same approach and performed a second, iterative ATAC-seq experiment to determine a second round of OCRs with greater accessibility in a subset of neurons. We then subcloned these second round OCRs so we could use *Gal4/FLP* intersectional genetics. This approach yielded new tools that were expressed in a subset of a set of neurons, showing that this iterative approach can be used to isolate increasingly specific cell populations. Compared to our first round of ATAC-seq from whole bodies and neurons (Fig. 1), we obtained many fewer differentially accessible OCRs when we compared pan-neuronal versus specific neuron ATAC-seq (Fig. 5). Thus, we only generated 2-s round *OCR2-FLP-transgene* lines to dissect the parental *2L722-Gal4* pattern. To more systematically dissect the *2L722* pattern, one could generate more second round transgenic lines and increase sequencing depth to identify additional differentially accessible OCRs to begin with. Furthermore, our FLP approach yielded more clonal intersectional patterns than hoped for. We used FLP because that approach is compatible with intersectional genetics using any parental Gal4 line. Alternatively, the split Gal4 system could be used for more reproducible intersectional patterns (*43*), but this approach would require *parent-Gal4* lines to be converted into *parent-split-Gal4* lines, which is not always straightforward. In general, however, an intersectional genetic approach to further subdivide a pre-existing expression pattern is also available in mammals using recombinases such as Cre or even FLP. Such an approach has been used in the mouse brain to co-inject and differentially/combinatorially label two distinct ATAC-seq-derived viruses (*42*). Our iterative ATAC-seq approach can thus be used to sequentially home in on decreasing subsets in a tissue of interest, and one could even perform a third iterative round of ATAC-seq data acquisition and OCR3 subcloning for additional specificity. Furthermore, tissue-specific ATAC-seq and intersectional strategies for in vivo expression are available from flies to mammals.

We also show that our approach can be used to isolate functionally relevant neurons. From our first round *OCR-Gal4* transgenes, more of the neuron-enriched lines affected sleep behavior than from the body-enriched ones (Fig. 4), as one might predict, given that the *neuron-OCR-Gal4* lines are more widely expressed in the brain than the *whole fly-OCR-Gal4* lines (Figs. 2 and 3). Our intersectional approach (Fig. 6) suggested that neurons in the lateral horn (Fig. 6, B and C) are involved in the nighttime sleep phenotype we observed in the parental *2L722-Gal4* line (Fig. 4). While we have not confirmed the identity of these putative sleep-regulating neurons, it is worth noting that some lateral horn neurons are involved in the regulation of sleep (*44*) and output from the circadian clock (*45*). Thus, our approach can be leveraged to identify and manipulate increasingly specific sets of neurons that are behaviorally relevant. The iterative nature of our approach represents a key step forward in the generation of increasingly cell type–specific tools and can be applied to any tissue of interest across the phylogenetic tree.

MATERIALS AND METHODS

Fly strains

The following fly lines were obtained from the Bloomington Drosophila Stock Center (Indiana University, Bloomington, IN, USA) and used

in this study: *Actin5c-Gal4* (BL25374), *Tubulin84B-Gal4* (BL5138), *elav-Gal4* (BL458), *nSyb-Gal4* (BL51635), *UAS-GFP-nls* (nuclear localization signal; BL4775), *UAS-Stinger* (a super-bright GFP-nls variant; BL84277), *UAS-mCD8::GFP* (BL32184), *UAS-myr::smGdP-V5* (BL62146), *UAS-LacZ* (BL1776), *UAS-TrpA1* (BL26263), *UAS-myr::GFP UAS-FRT-STOP-FRT-smHA* (BL62128), *UAS-FRT-STOP-FRT-TrpA1* (BL66871), and *w[*]; P{w[+mC] = Ubi-p63E(FRT.STOP) Stinger}9F6* (BL32250). Flies were reared in bottles containing standard cornmeal agar and grown at 25°C with 70% relative humidity and a 12-hour light/12-hour dark cycle.

ATAC-seq library construction

Flies containing *Tubulin84B-Gal4*, *Actin5c-Gal4*, *elav-Gal4*, or *nsyb-Gal4* drivers were used to induce nuclear GFP expression in whole flies or neurons. GFP-positive nuclei from approximately 250 flies per sample were isolated using our previously described workflow (*23*). Note that with sparser drivers, more flies will be needed to achieve the required input for ATAC-seq [50 to 60,000 nuclei per sample (*46*)]. The isolated nuclei were resuspended in 1 ml of wash buffer (10 mM tris-HCl, 10 mM NaCl, and 3 mM $MgCl_2$) containing 3 μM 4′,6-diamidino-2-phenylindole (DAPI) and were sorted using a BD FACSAria III flow cytometer (BD Biosciences, San Jose, CA, USA) operated by the University of Utah Flow Cytometry Core facility. GFP-negative nuclei collected from *w* Berlin* flies (no GFP) were stained with 3 μM DAPI and used as the GFP-negative control to set the sorting gates. Nuclei were identified on the basis of the forward scatter signal and DAPI intensity. GFP-positive nuclei were collected into 500 μl of wash buffer and stored on ice until use for ATAC-seq library prep. The purified nuclei were used for library preparation as previously described (*23*, *47*), with tagmentation for 23 min at 37°C using 1X Tn5 enzyme (Illumina Inc., San Diego, CA, USA). Fragments were amplified with Nextera index primers (Illumina) and Phusion HiFi master mix (New England Biolabs, Ipswich, MA, USA) for five cycles, followed by another 9 to 10 cycles per sample (as determined from 25% of total fluorescence from a quantitative polymerase chain reaction (PCR) side reaction performed using SsoFast EvaGreen SuperMix, Bio-Rad, Hercules, CA, USA). The DNA fragments were purified with 0.5X and 1.3X AMPure XP beads (Beckman Coulter, Indianapolis, IN, USA) to remove primer-dimers and high–molecular weight DNA (>5000 bp). The purified DNA was stored at −20°C until further analysis.

Sequencing and analysis

ATAC-seq libraries constructed using nuclei from whole flies (*Tubulin84B-Gal4* and *Actin5c-Gal4*) and head neurons (*elav-Gal4* and *nsyb-Gal4*) were sequenced on a HiSeq 2500 instrument using 50-bp paired-end reads. The fastq files were quality checked using FastQC (v 0.11.9). Adapter sequences were removed with CutAdapt (v3.4) (*48*). The sequenced reads were aligned to the dmel_r6.26 genome assembly using Bowtie2 (v2.4.2) (*49*). Aligned reads were sorted with Samtools (v1.12) (*50*) and deduplicated with Picard (v2.23) using the MarkDuplicates command. Aligned, filtered, and deduplicated reads were used to call peaks using MACS2 software (v2.2.5) (*51*). Differential accessibility analysis was performed using DiffBind (v2.10.0)(*52*) and DESeq2 (v1.32.0) (*53*). Peak annotation was performed using ChIPseeker (v1.30.3) (*54*). Coverage files were generated using DeepTools (v3.3.2) (*55*). Peaks were visualized using the IGV browser (v2.7.2) (*56*).

Plasmid construction

Unless otherwise stated, all restriction enzymes were from NEB. All PCR amplification steps were performed using Phusion High Fidelity PCR MasterMix (NEB) and the primers listed in table S1 (Invitrogen). Amplified fragments were purified from 1% agarose gels using Monarch DNA Gel Extraction Kits (NEB). A multiple cloning site (MCS; table S1) containing unique PacI, NheI, StuI, and AvrII restriction sites was designed and synthesized as a gBlock (Integrated DNA Technologies, Coralville, IA, USA). The MCS was subcloned into pENTR_D_TOPO (Thermo Fisher Scientific) and was inserted into pBPGw (17574, Addgene) using LR Clonase II (Thermo Fisher Scientific). The resulting plasmid (pBP-MCS-DSCP-Gal4; pMDG) was digested with AvrII and religated with T4 DNA ligase (NEB) to remove a 90-bp filler sequence within the MCS. To build pBP-MCS-Hsp70-Gal4 (pMHG), the 292-bp *Hsp70* promoter was amplified from pT-Arf6-T44N-GFP (an in-house plasmid) with the primers listed in table S1. The *HSP70* promoter was amplified, gel-purified, and subcloned into FseI/Kpn I–digested purified pMDG using NEBuilder HiFi DNA Assembly mix (NEB). pBP-MCS-DSCP-FlpD5 plasmid (pMDF) was constructed by amplifying the FlpD5 sequence from pBPhsFlp1 (32148, Addgene) with the primers listed in table S1. In parallel, pMDG was amplified with primers (table S1) designed to remove the Gal4 coding sequence. This yielded a linear backbone for FlpD5 insertion. The linear backbone and FlpD5 were assembled with NEBuilder HiFi DNA Assembly mix.

To construct plasmids containing *OCR*s, genomic DNA was purified from whole *w* Berlin* flies using Monarch Genomic DNA purification kits (NEB). *OCR*s with significantly increased accessibility in neurons and whole flies were selected using the following criteria: largest $\log_2$ fold change, distance >500 bp from the TSS, and *OCR* location within the first intron or within a promoter 2 to 3 kb from the TSS. *OCR* sequences plus 200-bp flanking regions were amplified from genomic DNA with primers that included 20-bp sequences complementary to the sequences upstream from the PacI and downstream from the AvrII sites in pMDG, pMHG, and pMDF (primer sequences in table S1). Amplified DNA fragments were gel-purified and subcloned into PacI/AvrII–digested and gel-purifed pMDG, pMHG, and pMDF using NEBuilder HiFi DNA Assembly mix (NEB). All plasmids were transformed into 5-alpha competent *Escherichia coli* (C2987U, NEB). The assembled plasmids were Sanger-sequenced to confirm correct assembly (GENEWIZ).

Fly injection

The *OCR* plasmids were injected into P{y[+t7.7] = nos-phiC31\int.NLS}X, y[1] sc[1] v[1] sev[21]; P{y[+t7.7] = CaryP}attP2 flies (BL25710). The *OCR2* plasmids were injected into y[1] v[1] P{y[+t7.7] = nos-phiC31\int.NLS}X; P{y[+t7.7] = CaryP}attP40 flies (BL25709). All injections were performed by Rainbow Transgenic Flies Inc.

OCR-Gal4 characterization

OCR-Gal4 flies were crossed to *UAS-Stinger* virgins. Adult progeny were examined for GFP expression using an Olympus SZX10 dissecting microscope equipped with an Olympus DP72 camera. Images were captured using Olympus cellSens software (RGB color mode, exposure time = 300 ms, and ISO sensitivity = 800). For each genotype, images from three different females were collected. GFP fluorescence in whole flies (excluding the head) was determined using ImageJ software. To corroborate the ImageJ analysis, each image

was printed in duplicate and assigned a random number, which resulted in six numbered images per genotype. One image per genotype was used to generate six image decks (11 images per deck). The decks were randomized and ranked by six blinded investigators. GFP intensity was ranked from low (1) to high (11).

LacZ staining

OCR-Gal4 flies were crossed to *UAS-LacZ* female virgins. Five- to 6-day-old progeny were collected and frozen at −80°C. Frozen flies were allowed to equilibrate to −15° to −16°C in a Leica CM1950 cryostat for at least 30 min. Then, whole flies were embedded in OCT cutting medium and sectioned at 30 μm. The sections were mounted on Superfrost Plus slides and incubated with 500 μl of 2% X-Gal (20 mg/ml in *N*,*N*′-dimethylformamide; X1001-5, Zymo Research, Irvine, CA, USA) in 40 ml of X-Gal staining solution {10 mM sodium phosphate buffer (pH 7.2), 150 mM NaCl, 1 mM $MgCl_2$, 10 mM $K_4[Fe^{II}(CN)_6]$, 10 mM $K_3[Fe^{III}(CN)_6]$, and 0.1% Triton X-100} overnight at 37°C. The slides were washed 3 times with 1X phosphate-buffered saline (PBS) and mounted with Prolong Diamond mounting medium (Thermo Fisher Scientific). The labeled sections were imaged with an Olympus CKX53 inverted microscope. The final images were reconstructed in Adobe Photoshop v23.1.1.

ATAC-seq library construction from OCR-Gal4 flies

ATAC-seq libraries were constructed from nuclei expressing *UAS-Stinger* driven by *3R579-Gal4* and *2L722-Gal4* (approximately 400 flies per sample). The nuclei were collected, and the ATAC-seq libraries were constructed as described (*23*, *47*). The libraries were sequenced with a NovaSeq 6000 instrument (Illumina) using 50-bp paired-end reads, and the resulting data were analyzed as described for the initial ATAC-seq libraries. OCRs with increased accessibility in *3R579-Gal4* and *2L722-Gal4* flies compared to *elav-Gal4* and *nSyb-Gal4* were selected by location in first introns, $\log_2$ fold change > 1, and adjusted $P < 0.05$. *OCR2*s were subcloned into pMDF as described above.

Immunofluorescence

OCR-Gal4 male flies were crossed to *UAS-myr::smGdP-V5* virgin females. Brains from 5–6 day old progeny were dissected in ice-cold PBS containing 0.5% Triton-X 100 (T-PBS) and placed in 4% paraformaldehyde (PFA) in PBS on ice. The brains were post-fixed for 20 min in fresh 4% PFA at room temperature on a nutator. After fixing, the tissue was washed 3 times with 0.5% T-PBS (20 min each), blocked for at least 30 min with 5% normal goat serum in 0.5% T-PBS, and incubated at 4°C for at least two nights with mouse anti-nc82 [1:20; catalog no. nc82, *Drosophila* Studies Hybridoma Bank (DSHB) at the University of Iowa, RRID: AB_2314866], Alexa Fluor 647–conjugated mouse anti-V5 (1:300; clone SV5-Pk1, catalog no. MCA1360A647, Bio-Rad, RRID: AB_770156), and rat anti-elav (1:700; clone 7E8A10, catalog no. Rat-Elav-7E8A10 anti-elav, DSHB, RRID:AB_528218) in 5% normal goat serum in 0.5% T-PBS. The brains were washed 3 times with 0.5% T-PBS and incubated for at least two nights in goat anti-mouse Alexa Fluor 488 (1:1000; catalog no. A11001, Thermo Fisher Scientific, RRID:AB_2534069) and goat anti-rat Alexa Fluor 594 (1:1000; catalog no. A11007, Thermo Fisher Scientific, RRID:AB_10561522). After labeling, the brains were washed with 0.5% T-PBS for 20 min and post-fixed in 4% PFA in PBS for 4 hours at room temperature on a nutator. The tissue was washed once in 0.5% T-PBS and 3 times in 1X PBS (15 min each) and mounted on Superfrost Plus slides (VWR). The brains were dehydrated in 30, 50, 75, 95, and 3 times 100% ethanol for 10 min each. The slides were cleared 3 times in xylene (5 min each) and mounted with DPX (Sigma-Aldrich).

Male flies containing *OCR2*s (*OCR2-Flp;2L722-Gal4*) were crossed to *UAS-myr::GFP-FRT-STOP-FRT-smHA* or *Ubi-p63E(FRT.STOP) Stinger* female virgins for 24 hours. The flies were flipped into a new vial and were allowed to mate and lay eggs for 24 hours. The parental flies were removed, and the seeded vials were incubated at 25°C for 24 hours to allow eggs to hatch and the larvae to develop to the first instar stage. The first-instar larvae were heat shocked at 37°C for 1 hour in a water bath. Twenty-four hours later, the larvae were heat-shocked again and allowed to recover for another 24 hours. The larvae were heat-shocked a third time and allowed to develop normally afterward. Brains were dissected and stained as described above using mouse anti-nc82 (1:20), chicken anti-GFP (1:500; catalog no. AB16901; MilliporeSigma, RRID:AB_90890), Alexa Fluor 647–conjugated mouse anti-HA (1:300, clone 6E2, catalog no. 3444S, Cell Signaling Technology, Danvers, MA, USA) or Alexa Fluor 647–conjugated mouse anti-V5 and rat anti-elav (1:700). Secondary antibodies were goat anti-mouse Alexa Fluor 488 (1:1000; Thermo Fisher Scientific), goat anti-chicken Alexa Fluor Plus 594 (1:1000; catalog no. A32759, Thermo Fisher Scientific), and goat anti-rat Alexa Fluor 594 (1:1000). Immunostained brains were washed, post-fixed, and mounted as described above. All immunolabeled brains were imaged using the Leica SP8 white light laser confocal microscope at the University of Utah HSC Cell Imaging Core Facility. All images were processed using the Fiji distribution of ImageJ (v2.3.0/1.53q) (*57*).

Sleep experiments

For sleep experiments, *OCR-Gal4* male flies were crossed to *UAS-TrpA1* female virgins. *OCR2-Flp;2L722-Gal4* male flies were crossed to *UAS-FRT-STOP-FRT-TrpA1* female virgin flies. The *OCR2*-expressing progeny were heat shocked to induce Flp activity as described above. Fly locomotor activity was monitored using the Drosophila Activity Monitor system (DAM3, Trikinetics, Waltham, MA). Flies were individually loaded into 65-mm glass tubes and placed within the DAM system. Flies were kept in an incubator with a 12-hour light/12-hour dark cycle. Behavior was recorded for 2 days at 21°C. Then, the temperature was shifted to 29°C and activity was recorded for two more days. The sleep data were quantified using custom software (*58*) in MATLAB (MathWorks, Natick, MA). The data obtained for each sleep parameter at 21°C were subtracted from the data from the same fly obtained at 29°C before statistical analysis.

Statistical analysis

Statistical analysis was performed in GraphPad 9 (version 9.4.1) or R (version 4.2.1) software. Annotated feature proportions were analyzed using Mann-Whitney *U* tests (whole flies versus head neurons; Fig. 1B) or Kruskal-Wallis tests followed by Dunn's multiple comparisons tests (head neurons versus *2L722* or *3R579* neurons; Fig. 5C). GFP fluorescence intensity (Fig. 2) and reporter immunostaining (Fig. 3) were analyzed using Wilcoxon signed-rank tests. Differences in nighttime sleep were analyzed using Kruskal-Wallis tests followed by Dunn's multiple comparisons test. Reporter labeling in Fig. 6 and fig. S4 was ranked by blinded investigators. The frequency of staining for each pattern was calculated and compared using Chi-squared tests. Differences were considered statistically significant at $P < 0.05$. Sample sizes for all experiments are shown in table S2.

Supplementary Materials

This PDF file includes:
Figs. S1 and S7
Legends for tables S1 and S2

Other Supplementary Material for this manuscript includes the following:
Tables S1 and S2

REFERENCES AND NOTES

1. R. Yuste, From the neuron doctrine to neural networks. *Nat. Rev. Neurosci.* **16**, 487–497 (2015).
2. C. Liu, P. Y. Plaçais, N. Yamagata, B. D. Pfeiffer, Y. Aso, A. B. Friedrich, I. Siwanowicz, G. M. Rubin, T. Preat, H. Tanimoto, A subset of dopamine neurons signals reward for odour memory in Drosophila. *Nature* **488**, 512–516 (2012).
3. Y. Aso, D. Hattori, Y. Yu, R. M. Johnston, N. A. Iyer, T. T. B. Ngo, H. Dionne, L. F. Abbott, R. Axel, H. Tanimoto, G. M. Rubin, The neuronal architecture of the mushroom body provides a logic for associative learning. *eLife* **3**, e04577–e04577 (2014).
4. L. K. Scheffer, C. S. Xu, M. Januszewski, Z. Lu, S.-Y. Takemura, K. J. Hayworth, G. B. Huang, K. Shinomiya, J. Maitlin-Shepard, S. Berg, J. Clements, P. M. Hubbard, W. T. Katz, L. Umayam, T. Zhao, D. Ackerman, T. Blakely, J. Bogovic, T. Dolafi, D. Kainmueller, T. Kawase, K. A. Khairy, L. Leavitt, P. H. Li, L. Lindsey, N. Neubarth, D. J. Olbris, H. Otsuna, E. T. Trautman, M. Ito, A. S. Bates, J. Goldammer, T. Wolff, R. Svirskas, P. Schlegel, E. Neace, C. J. Knecht, C. X. Alvarado, D. A. Bailey, S. Ballinger, J. A. Borycz, B. S. Canino, N. Cheatham, M. Cook, M. Dreher, O. Duclos, B. Eubanks, K. Fairbanks, S. Finley, N. Forknall, A. Francis, G. P. Hopkins, E. M. Joyce, S. Kim, N. A. Kirk, J. Kovalyak, S. A. Lauchie, A. Lohff, C. Maldonado, E. A. Manley, S. McLin, C. Mooney, M. Ndama, O. Ogundeyi, N. Okeoma, C. Ordish, N. Padilla, C. M. Patrick, T. Paterson, E. E. Phillips, E. M. Phillips, N. Rampally, C. Ribeiro, M. K. Robertson, J. T. Rymer, S. M. Ryan, M. Sammons, A. K. Scott, A. L. Scott, A. Shinomiya, C. Smith, K. Smith, N. L. Smith, M. A. Sobeski, A. Suleiman, J. Swift, S. Takemura, I. Talebi, D. Tarnogorska, E. Tenshaw, T. Tokhi, J. J. Walsh, T. Yang, J. A. Horne, F. Li, R. Parekh, P. K. Rivlin, V. Jayaraman, M. Costa, G. S. Jefferis, K. Ito, S. Saalfeld, R. George, I. A. Meinertzhagen, G. M. Rubin, H. F. Hess, V. Jain, S. M. Plaza, A connectome and analysis of the adult Drosophila central brain. *eLife* **9**, e57443 (2020).
5. B. D. Pfeiffer, A. Jenett, A. S. Hammonds, T. T. B. Ngo, S. Misra, C. Murphy, A. Scully, J. W. Carlson, K. H. Wan, T. R. Laverty, C. Mungall, R. Svirskas, J. T. Kadonaga, C. Q. Doe, M. B. Eisen, S. E. Celniker, G. M. Rubin, Tools for neuroanatomy and neurogenetics in Drosophila. *Proc. Natl. Acad. Sci. U.S.A.* **105**, 9715–9720 (2008).
6. A. Jenett, G. M. Rubin, T. T. B. Ngo, D. Shepherd, C. Murphy, H. Dionne, B. D. Pfeiffer, A. Cavallaro, D. Hall, J. Jeter, N. Iyer, D. Fetter, J. H. Hausenfluck, H. Peng, E. T. Trautman, R. R. Svirskas, E. W. Myers, Z. R. Iwinski, Y. Aso, G. M. DePasquale, A. Enos, P. Hulamm, S. C. B. Lam, H. H. Li, T. R. Laverty, F. Long, L. Qu, S. D. Murphy, K. Rokicki, T. Safford, K. Shaw, J. H. Simpson, A. Sowell, S. Tae, Y. Yu, C. T. Zugates, A GAL4-driver line resource for Drosophila neurobiology. *Cell Rep.* **2**, 991–1001 (2012).
7. G. Farkas, B. A. Leibovitch, S. C. R. Elgin, Chromatin organization and transcriptional control of gene expression in Drosophila. *Gene* **253**, 117–136 (2000).
8. T. T. Marstrand, J. D. Storey, Identifying and mapping cell-type-specific chromatin programming of gene expression. *Proc. Natl. Acad. Sci. U.S.A.* **111**, E645–E654 (2014).
9. Y. Gui, K. Grzyb, M. H. Thomas, J. Ohnmacht, P. Garcia, M. Buttini, A. Skupin, T. Sauter, L. Sinkkonen, Single-nuclei chromatin profiling of ventral midbrain reveals cell identity transcription factors and cell-type-specific gene regulatory variation. *Epigenetics Chromatin* **14**, 1–20 (2021).
10. C. M. Palmateer, S. C. Moseley, S. Ray, S. G. Brovero, M. N. Arbeitman, Analysis of cell-type-specific chromatin modifications and gene expression in Drosophila neurons that direct reproductive behavior. *PLOS Genet.* **17**, e1009240–e1009240 (2021).
11. A. Rotem, O. Ram, N. Shoresh, R. A. Sperling, A. Goren, D. A. Weitz, B. E. Bernstein, Single-cell ChIP-seq reveals cell subpopulations defined by chromatin state. *Nat. Biotechnol.* **33**, 1165–1172 (2015).
12. W. Winick-Ng, A. Kukalev, I. Harabula, L. Zea-Redondo, D. Szabo, M. Meijer, L. Serebreni, Y. Zhang, S. Bianco, A. M. Chiariello, I. Irastorza-Azcarate, C. J. Thieme, T. M. Sparks, S. Carvalho, L. Fiorillo, F. Musella, E. Irani, E. Torlai Triglia, A. A. Kolodziejczyk, A. Abentung, G. Apostolova, E. J. Paul, V. Franke, R. Kempfer, A. Akalin, S. A. Teichmann, G. Dechant, M. A. Ungless, M. Nicodemi, L. Welch, G. Castelo-Branco, A. Pombo, Cell-type specialization is encoded by specific chromatin topologies. *Nature* **599**, 684–691 (2021).
13. J. D. Buenrostro, P. G. Giresi, L. C. Zaba, H. Y. Chang, W. J. Greenleaf, Transposition of native chromatin for fast and sensitive epigenomic profiling of open chromatin, DNA-binding proteins and nucleosome position. *Nat. Methods* **10**, 1213–1218 (2013).
14. A. M. Ackermann, Z. Wang, J. Schug, A. Naji, K. H. Kaestner, Integration of ATAC-seq and RNA-seq identifies human alpha cell and beta cell signature genes. *Mol. Metab.* **5**, 233–244 (2016).
15. I. Grbesa, M. Tannenbaum, A. Sarusi-Portuguez, M. Schwartz, O. Hakim, Mapping genome-wide accessible chromatin in primary human T lymphocytes by ATAC-seq. *J. Vis. Exp.* **2017**, 56313–56313 (2017).
16. J. Wang, C. Zibetti, P. Shang, S. R. Sripathi, P. Zhang, M. Cano, T. Hoang, S. Xia, H. Ji, S. L. Merbs, D. J. Zack, J. T. Handa, D. Sinha, S. Blackshaw, J. Qian, ATAC-Seq analysis reveals a widespread decrease of chromatin accessibility in age-related macular degeneration. *Nat. Comm.* **9**, 1–13 (2018).
17. M. Bysani, R. Agren, C. Davegårdh, P. Volkov, T. Rönn, P. Unneberg, K. Bacos, C. Ling, ATAC-seq reveals alterations in open chromatin in pancreatic islets from subjects with type 2 diabetes. *Sci. Rep.* **9**, 7785 (2019).
18. S. Fujiwara, S. Baek, L. Varticovski, S. Kim, G. L. Hager, High quality ATAC-seq data recovered from cryopreserved breast cell lines and tissue. *Sci. Rep.* **9**, 1–11 (2019).
19. J. R. Sinnamon, K. A. Torkenczy, M. W. Linhoff, S. A. Vitak, R. M. Mulqueen, H. A. Pliner, C. Trapnell, F. J. Steemers, G. Mandel, A. C. Adey, The accessible chromatin landscape of the murine hippocampus at single-cell resolution. *Genome Res.* **29**, 857–869 (2019).
20. B. Aydin, A. Kakumanu, M. Rossillo, M. Moreno-Estellés, G. Garipler, N. Ringstad, N. Flames, S. Mahony, E. O. Mazzoni, Proneural factors Ascl1 and Neurog2 contribute to neuronal subtype identities by establishing distinct chromatin landscapes. *Nat. Neurosci.* **22**, 897–908 (2019).
21. J. Janssens, S. Aibar, I. I. Taskiran II, J. N. Ismail, A. E. Gomez, G. Aughey, K. I. Spanier, F. V. De Rop, C. B. Gonzalez-Blas, M. Dionne, K. Grimes, X. J. Quan, D. Papasokrati, G. Hulselmans, S. Makhzami, M. De Waegeneer, V. Christiaens, T. Southall, S. Aerts, Decoding gene regulation in the fly brain. *Nature* **601**, 630–636 (2022).
22. A. H. Brand, N. Perrimon, Targeted gene expression as a means of altering cell fates and generating dominant phenotypes. *Development* **118**, 401–415 (1993).
23. C. B. Merrill, M. A. Pabon, A. B. Montgomery, A. R. Rodan, A. Rothenfluh, Optimized assay for transposase-accessible chromatin by sequencing (ATAC-seq) library preparation from adult Drosophila melanogaster neurons. *Sci. Rep.* **12**, 6043 (2022).
24. S. Roy, J. Ernst, P. V. Kharchenko, P. Kheradpour, N. Negre, M. L. Eaton, J. M. Landolin, C. A. Bristow, L. Ma, M. F. Lin, S. Washietl, B. I. Arshinoff, F. Ay, P. E. Meyer, N. Robine, N. L. Washington, L. Di Stefano, E. Berezikov, C. D. Brown, R. Candeias, J. W. Carlson, A. Carr, I. Jungreis, D. Marbach, R. Sealfon, M. Y. Tolstorukov, S. Will, A. A. Alekseyenko, C. Artieri, B. W. Booth, A. N. Brooks, Q. Dai, C. A. Davis, M. O. Duff, X. Feng, A. A. Gorchakov, T. Gu, J. G. Henikoff, P. Kapranov, R. Li, H. K. MacAlpine, J. Malone, A. Minoda, J. Nordman, K. Okamura, M. Perry, S. K. Powell, N. C. Riddle, A. Sakai, A. A. Samsonova, J. E. Sandler, Y. B. Schwartz, N. Sher, R. Spokony, D. Sturgill, M. van Baren, K. H. Wan, L. Yang, C. Yu, E. Feingold, P. Good, M. Guyer, R. Lowdon, K. Ahmad, J. Andrews, B. Berger, S. E. Brenner, M. R. Brent, L. Cherbas, S. C. R. Elgin, T. R. Gingeras, R. Grossman, R. A. Hoskins, T. C. Kaufman, W. Kent, M. I. Kuroda, T. Orr-Weaver, N. Perrimon, V. Pirrotta, J. W. Posakony, B. Ren, S. Russell, P. Cherbas, B. R. Graveley, S. Lewis, G. Micklem, B. Oliver, P. J. Park, S. E. Celniker, S. Henikoff, G. H. Karpen, E. C. Lai, D. M. MacAlpine, L. D. Stein, K. P. White, M. Kellis, B. Booth, C. L. G. Comstock, A. Dobin, J. Drenkow, S. Dudoit, J. Dumais, D. Fagegaltier, S. Ghosh, K. D. Hansen, S. Jha, L. Langton, W. Lin, D. Miller, A. E. Tenney, H. Wang, A. T. Willingham, C. Zaleski, D. Zhang, D. Acevedo, E. P. Bishop, S. E. Gadel, Y. L. Jung, C. D. Kennedy, O. K. Lee, D. Linder-Basso, S. E. Marchetti, G. Shanower, N. Nègre, R. L. Grossman, R. Auburn, H. J. Bellen, J. Chen, M. H. Domanus, D. Hanley, E. Heinz, Z. Li, F. Meyer, S. W. Miller, C. A. Morrison, D. A. Scheftner, L. Senderowicz, P. K. Shah, S. Suchy, F. Tian, K. J. T. Venken, R. White, J. Wilkening, J. Zieba, J. T. Nordman, T. L. Orr-Weaver, L. C. DeNapoli, Q. Ding, T. Eng, H. Kashevsky, S. Li, J. A. Prinz, G. J. Hannon, M. Hirst, M. Marra, M. Rooks, Y. Zhao, T. D. Bryson, M. D. Perry, W. J. Kent, S. E. Lewis, G. Barber, A. Chateigner, H. Clawson, S. Contrino, F. Guillier, A. S. Hinrichs, E. T. Kephart, P. Lloyd, R. Lyne, S. McKay, R. A. Moore, C. Mungall, K. M. Rutherford, P. Ruzanov, R. Smith, E. O. Stinson, Z. Zha, C. G. Artieri, J. H. Malone, L. Jiang, N. Mattiuzzo, E. A. Feingold, P. J. Good, M. S. Guyer, R. F. Lowdon, Identification of functional elements and regulatory circuits by Drosophila modENCODE. *Science* **330**, 1787–1797 (2010).
25. S. S. Gisselbrecht, A. Palagi, J. V. Kurland, J. M. Rogers, H. Ozadam, Y. Zhan, J. Dekker, M. L. Bulyk, Transcriptional silencers in Drosophila serve a dual role as transcriptional enhancers in alternate cellular contexts. *Mol. Cell* **77**, 324–337.e8 (2020).
26. J. Bischof, R. K. Maeda, M. Hediger, F. Karch, K. Basler, An optimized transgenesis system for Drosophila using germ-line-specific φC31 integrases. *Proc. Natl. Acad. Sci. U.S.A.* **104**, 3312–3317 (2007).
27. T. O'Brien, J. T. Lis, Rapid changes in Drosophila transcription after an instantaneous heat shock. *Mol. Cell. Biol.* **13**, 3456–3463 (1993).
28. A. Nern, B. D. Pfeiffer, G. M. Rubin, Optimized tools for multicolor stochastic labeling reveal diverse stereotyped cell arrangements in the fly visual system. *Proc. Natl. Acad. Sci. U.S.A.* **112**, E2967–E2976 (2015).
29. F. N. Hamada, M. Rosenzweig, K. Kang, S. R. Pulver, A. Ghezzi, T. J. Jegla, P. A. Garrity, An internal thermal sensor controlling temperature preference in Drosophila. *Nature* **454**, 217–220 (2008).
30. J. M. Donlea, D. Pimentel, G. Miesenböck, Neuronal machinery of sleep homeostasis in Drosophila. *Neuron* **81**, 860–872 (2014).
31. F. Guo, J. Yu, H. J. Jung, K. C. Abruzzi, W. Luo, L. C. Griffith, M. Rosbash, Circadian neuron feedback controls the Drosophila sleep–activity profile. *Nature* **536**, 292–297 (2016).
32. N. A. Shalaby, J. H. Pinzon, A. S. Narayanan, E. J. Jin, M. P. Ritz, R. J. Dove, H. Wolfenberg, A. R. Rodan, M. Buszczak, A. Rothenfluh, JmjC domain proteins modulate circadian behaviors and sleep in Drosophila. *Sci. Rep.* **8**, 815 (2018).

33. O. T. Shafer, A. C. Keene, The regulation of Drosophila sleep. *Curr. Biol.* **31**, R38–R49 (2021).
34. Y. E. Fisher, H. H. Yang, J. Isaacman-Beck, M. Xie, D. M. Gohl, T. R. Clandinin, FlpStop, a tool for conditional gene control in Drosophila. *eLife* **6**, e22279 (2017).
35. J. B. Duffy, D. A. Harrison, N. Perrimon, Identifying loci required for follicular patterning using directed mosaics. *Development* **125**, 2263–2271 (1998).
36. S. S. Blair, Genetic mosaic techniques for studying Drosophila development. *Development* **130**, 5065–5072 (2003).
37. S. Blankvoort, M. P. Witter, J. Noonan, J. Cotney, C. Kentros, Marked diversity of unique cortical enhancers enables neuron-specific tools by enhancer-driven gene expression. *Curr. Biol.* **28**, 2103–2114.e5 (2018).
38. X. Zhu, S. M. Ahmad, A. Aboukhalil, B. W. Busser, Y. Kim, T. R. Tansey, A. Haimovich, N. Jeffries, M. L. Bulyk, A. M. Michelson, Differential regulation of mesodermal gene expression by Drosophila cell type-specific Forkhead transcription factors. *Development* **139**, 1457–1466 (2012).
39. M. Bozek, R. Cortini, A. E. Storti, U. Unnerstall, U. Gaul, N. Gompel, ATAC-seq reveals regional differences in enhancer accessibility during the establishment of spatial coordinates in the Drosophila blastoderm. *Genome Res.* **29**, 771–783 (2019).
40. Y.-C. D. Chen, Y.-C. Chen, R. Rajesh, N. Shoji, M. Jacy, H. Lacin, T. Erclik, C. Desplan, Using single-cell RNA sequencing to generate predictive cell-type-specific split-GAL4 reagents throughout development. *Proc. Natl. Acad. Sci. U.S.A.* **120**, e2307451120 (2023).
41. S. Hrvatin, C. P. Tzeng, M. A. Nagy, H. Stroud, C. Koutsioumpa, O. F. Wilcox, E. G. Assad, J. Green, C. D. Harvey, E. C. Griffith, M. E. Greenberg, A scalable platform for the development of cell-type-specific viral drivers. *eLife* **8**, e48089 (2019).
42. L. T. Graybuck, T. L. Daigle, A. E. Sedeño-Cortés, M. Walker, B. Kalmbach, G. H. Lenz, E. Morin, T. N. Nguyen, E. Garren, J. L. Bendrick, T. K. Kim, T. Zhou, M. Mortrud, S. Yao, L. A. Siverts, R. Larsen, B. B. Gore, E. R. Szelenyi, C. Trader, P. Balaram, C. T. J. Van Velthoven, M. Chiang, J. K. Mich, N. Dee, J. Goldy, A. H. Cetin, K. Smith, S. W. Way, L. Esposito, Z. Yao, V. Gradinaru, S. M. Sunkin, E. Lein, B. P. Levi, J. T. Ting, H. Zeng, B. Tasic, Enhancer viruses for combinatorial cell-subclass-specific labeling. *Neuron* **109**, 1449–1464.e13 (2021).
43. H. Luan, F. Diao, R. L. Scott, B. H. White, The Drosophila Split Gal4 system for neural circuit mapping. *Front. Neural Circuits* **14**, 603397 (2020).
44. C. T. Hsu, J. T. Y. Choi, A. Sehgal, Manipulations of the olfactory circuit highlight the role of sensory stimulation in regulating sleep amount. *Sleep* **44**, zsaa265 (2021).
45. M. Cavey, B. Collins, C. Bertet, J. Blau, Circadian rhythms in neuronal activity propagate through output circuits. *Nat. Neurosci.* **19**, 587–595 (2016).
46. J. D. Buenrostro, B. Wu, H. Y. Chang, W. J. Greenleaf, "ATAC-seq: A method for assaying chromatin accessibility genome-wide" in *Current Protocols in Molecular Biology* (John Wiley & Sons Inc., 2015), vol. 109, 21.29.21–21.29.29.
47. M. R. Corces, A. E. Trevino, E. G. Hamilton, P. G. Greenside, N. A. Sinnott-Armstrong, S. Vesuna, A. T. Satpathy, A. J. Rubin, K. S. Montine, B. Wu, A. Kathiria, S. W. Cho, M. R. Mumbach, A. C. Carter, M. Kasowski, L. A. Orloff, V. I. Risca, A. Kundaje, P. A. Khavari, T. J. Montine, W. J. Greenleaf, H. Y. Chang, An improved ATAC-seq protocol reduces background and enables interrogation of frozen tissues. *Nat. Methods* **14**, 959–962 (2017).
48. M. Martin, Cutadapt removes adapter sequences from high-throughput sequencing reads. *EMBnet J.* **17**, 10–10 (2011).
49. B. Langmead, S. L. Salzberg, Fast gapped-read alignment with Bowtie 2. *Nat. Methods* **9**, 357–359 (2012).
50. H. Li, B. Handsaker, A. Wysoker, T. Fennell, J. Ruan, N. Homer, G. Marth, G. Abecasis, R. Durbin, The Sequence Alignment/Map format and SAMtools. *Bioinformatics* **25**, 2078–2079 (2009).
51. Y. Zhang, T. Liu, C. A. Meyer, J. Eeckhoute, D. S. Johnson, B. E. Bernstein, C. Nussbaum, R. M. Myers, M. Brown, W. Li, X. S. Liu, Model-based analysis of ChIP-Seq (MACS). *Genome Biol.* **9**, R137–R137 (2008).
52. C. S. Ross-Innes, R. Stark, A. E. Teschendorff, K. A. Holmes, H. R. Ali, M. J. Dunning, G. D. Brown, O. Gojis, I. O. Ellis, A. R. Green, S. Ali, S. F. Chin, C. Palmieri, C. Caldas, J. S. Carroll, Differential oestrogen receptor binding is associated with clinical outcome in breast cancer. *Nature* **481**, 389–393 (2012).
53. M. I. Love, W. Huber, S. Anders, Moderated estimation of fold change and dispersion for RNA-seq data with DESeq2. *Genome Biol.* **15**, 1–21 (2014).
54. G. Yu, L.-G. Wang, Q.-Y. He, ChIPseeker: An R/Bioconductor package for ChIP peak annotation, comparison and visualization. *Bioinformatics* **31**, 2382–2383 (2015).
55. F. Ramirez, D. P. Ryan, B. Gruning, V. Bhardwaj, F. Kilpert, A. S. Richter, S. Heyne, F. Dundar, T. Manke, deepTools2: A next generation web server for deep-sequencing data analysis. *Nucleic Acids Res.* **44**, W160–W165 (2016).
56. J. T. Robinson, H. Thorvaldsdóttir, W. Winckler, M. Guttman, E. S. Lander, G. Getz, J. P. Mesirov, Integrative genomics viewer. *Nat. Biotechnol.* **29**, 24–26 (2011).
57. J. Schindelin, I. Arganda-Carreras, E. Frise, V. Kaynig, M. Longair, T. Pietzsch, S. Preibisch, C. Rueden, S. Saalfeld, B. Schmid, J. Y. Tinevez, D. J. White, V. Hartenstein, K. Eliceiri, P. Tomancak, A. Cardona, Fiji: An open-source platform for biological-image analysis. *Nat. Methods* **9**, 676–682 (2012).
58. A. Vaccaro, Y. Kaplan Dor, K. Nambara, E. A. Pollina, C. Lin, M. E. Greenberg, D. Rogulja, Sleep loss can cause death through accumulation of reactive oxygen species in the gut. *Cell* **181**, 1307–1328.e15 (2020).

Acknowledgments: We thank members of the A.R. and A.R.R. laboratories for discussion. We acknowledge the Cell Imaging Core at the University of Utah for use of equipment (Leica SP8 White Light laser confocal microscope). Stocks obtained from the Bloomington *Drosophila* Stock Center (NIH P40OD018537) were used in this study. This work was supported by the University of Utah Flow Cytometry Facility, the University of Utah Genomics Core Facility, the High Throughput Sequencing Core at the Huntsman Cancer Institute, and the National Cancer Institute through award number 5P30CA042014. **Funding:** This work was supported by the National Institute on Drug Abuse Grant R21DA049635 (to A.R.); National Institute on Alcohol Abuse and Alcoholism Grants K01AA029200 (to C.B.M.), R01AA026818 (to A.R.), R01AA019526 (to A.R.), and R01AA030881 (to A.R.); and National Institute of Diabetes and Digestive and Kidney Disease Grant R01DK110358 (to A.R.R.). **Author contributions:** Conceptualization: C.B.M. and A.R. Formal analysis: C.B.M., I.T., A.B.M., and A.R. Investigation: C.B.M., I.T., and M.A.P. Resources: M.A.P. Data curation: C.B.M. and A.B.M. Writing—original draft: C.B.M. and I.T. Writing—review and editing: C.B.M., I.T., M.A.P., A.R.R., and A.R. Visualization: C.B.M. Supervision: A.R. Funding acquisition: C.B.M., A.R.R., and A.R. **Competing interests:** The authors declare that they have no competing interests. **Data and materials availability:** All sequencing data are deposited in the Gene Expression Omnibus database (accession number: GSE226514). All generated plasmids and fly lines are available upon request. All data needed to evaluate the conclusions in the paper are present in the paper and/or the Supplementary Materials.

Submitted 25 April 2023
Accepted 21 February 2024
Published 27 March 2024
10.1126/sciadv.adi4393